Research Article

Lishan Tan, Xiulong Deng, Xuandi Lai, Tao Zeng, Aiqing Li*, Jianqiang Hu*, Zuying Xiong*

Mesoscale nanoparticles encapsulated with emodin for targeting antifibrosis in animal models

https://doi.org/10.1515/chem-2020-0163
received July 05, 2020; accepted August 17, 2020

Abstract: The aim of this study is to explore the kidney-targeting capability of mesoscale nanoparticles (MNPs)-emodin (Em-MNPs) and its potential antifibrosis in the animal model. First, MNPs and Em-MNPs were synthesized via nanoprecipitation method, and their diameters were both ~400 nm with the uniform size. The entrapment efficiency of MNPs was 45.1% when adding emodin at the concentration of 12 mg/mL. Moreover, cytotoxicity assay showed that Em-MNPs presented excellent biocompatibility in rat proximal tubular cells. Cellular uptake assay demonstrated that Em-MNPs had high-efficiency uptake, especially in the cytoplasm. *Ex vivo* organ fluorescence imaging revealed that Em-MNPs possessed specific kidney-targeting ability with relative long retention time in the kidney (~24 h). In the renal unilateral ureteral obstruction model, Em-MNPs treatment could significantly alleviate kidney tubule injury and reduce extracellular matrix deposition compared with free MNPs. Herein, Em-MNPs with specific kidney-targeting and preferable antifibrosis effects in animal model may pave an avenue for treating renal diseases.

Keywords: mesoscale nanoparticles, emodin, kidney-targeting, anti-fibrosis, UUO model

1 Introduction

Multifunctional nanomaterials have been widely studied in the biomedical field because of their unique and adjustable physicochemical properties [1]. Researches focused on their application in biosensor, bioimaging and diagnosis, drug delivery, and disease treatment, and tissue regeneration engineering have attracted widespread attention [2–5]. The biological functions and applications of nanomaterials are usually closely related to their structure, size, and surface chemistry (such as surface modification) [6,7]. Thus, appropriate construction and modification of nanomaterials are of significance to broaden their application. It is well known that shortcomings such as insufficient water solubility, no renal targeting, and high toxicity of some small molecule drugs often restricted the therapy efficiency in a variety of diseases. Therefore, it is urgent to develop nontoxic and specific targeting drug delivery system.

Chronic kidney disease (CKD) have attracted increasing worldwide attention because of its high morbidity (10.8%), and it often progresses to end-stage kidney disease (ESKD), which required renal replacement therapy [8]. The key procedure of CKD to ESKD is renal fibrosis [9], so finding the drugs to reverse or halt the progression of fibrosis is incredibly essential for CKD patients. Although the therapies of chronic fibrosis increased, there are several adverse effects in their clinical practice. Several ingredients of Chinese herbs

* **Corresponding author: Aiqing Li,** Department of Nephrology, State Key Laboratory of Organ Failure Research, Nanfang Hospital, Southern Medical University, Guangzhou, Guangdong, 510515, China, e-mail: liaiqing@smu.edu.cn
* **Corresponding author: Jianqiang Hu,** Department of Chemistry, Nanobiological Medicine Center, Key Lab of Fuel Cell Technology of Guangdong Province, School of Chemistry and Chemical Engineering, South China University of Technology, Guangzhou, Guangdong, 510640, China, e-mail: jqhusc@scut.edu.cn
* **Corresponding author: Zuying Xiong,** Department of Nephrology, Peking University Shenzhen Hospital, Shenzhen Peking University-The Hong Kong University of Science and Technology Medical Center, Shenzhen, Guangdong, 518036, China, e-mail: xiongzy2005@163.com
Lishan Tan: Department of Nephrology, Peking University Shenzhen Hospital, Shenzhen Peking University-The Hong Kong University of Science and Technology Medical Center, Shenzhen, Guangdong, 518036, China
Xiulong Deng: Department of Chemical and Chemical Engineering, Key Laboratory of Organo-Pharmaceutical Chemistry, Gannan Normal University, Ganzhou, Jiangxi Province, 341000, China
Xuandi Lai: Department of Oncology, Peking University Shenzhen Hospital, Shenzhen, Guangdong, 518036, China
Tao Zeng: Department of Nephrology, State Key Laboratory of Organ Failure Research, Nanfang Hospital, Southern Medical University, Guangzhou, Guangdong, 510515, China

(emodin and triptolide) that were verified have been useful in treating chronic kidney fibrosis [10–12]. However, they also have some disadvantages such as low aqueous solubility, low kidney targeting, and short retention that may limit their application [13]. Recently, several studies focus on the medical application of nanomaterials, such as gold nanoparticles (NPs), polymer NPs, and other NPs with different sizes [14,15]. Qiao et al. synthesized catechol-derived chitosan complex (HCA-Chi) to improve the water solubility and renal-targeting ability of emodin and to further alleviate chronic kidney injury, which was an effective way to increase the effects of Chinese herbs [16]. However, the retention time of HCA-Chi in the kidneys was relatively short (~12 h), and it would be preferable to prolong the kidney distribution time with good biocompatibility. Recently, it was demonstrated that mesoscale nanoparticles (MNPs), with a diameter of ~400 nm, showed excellent kidney targeting ability, high stability, and high efficiency for the treatment of acute kidney injury after loading triptolide [17]. Therefore, MNPs would be a potential nanoplatform for emodin delivery to the kidney and finally to improve chronic kidney fibrosis.

In this study, we constructed monodispersed MNPs and loaded with emodin (Em-MNPs, ~400 nm) for treating kidney fibrosis. Em-MNPs with good biocompatibility, kidney-targeting ability, and high uptake efficiency of kidney cells were synthesized for further pharmacodynamics study. Finally, we revealed that Em-MNPs had good therapeutic effects in the renal fibrosis animal model.

2 Materials and methods

2.1 Chemicals

Poly(D,L-lactate-*co*-glycolic acid) (PLGA; terminal carboxylation, molecular weight 38–54 kDa), EDC, methoxypolyethylene glycol amine (mPEG-NH_2, 5 kDa), and FBS were purchased from Sigma (USA). Emodin (Em), poloxam 188, acetonitrile, methanol, and ethyl acetate were purchased from Aladdin (Shanghai). Cy7 was purchased from Lumiprode (USA). Other chemical reagents were purchased from Sinopharm Group Chemical Reagent Co. LTD. Ultrapure water was used throughout the experiments (18.2 MΩ cm).

2.2 Fabrication of PLGA-b-mPEG

The synthesis of PLGA-b-mPEG was based on the method reported in the previous study [18], that is, it was synthesized by the amide reaction between the amino group of mPEG-NH_2 terminal and the carboxyl group of PLGA terminal. First, PLGA (1 g), mPEG-NH_2 (250 mg), and EDC (75 mg) were dissolved in 5 mL anhydrous chloroform and stirred vigorously at room temperature for 12 h. After the reaction, 15 mL ethyl ether/methanol mixture (V/V, 1:1, 0°C) was added to precipitate the product. Centrifugation (10,000 rpm, 15 min) was performed to collect the bottom residue, and the upper liquid was rotated to evaporate and then the solvent was removed. Then, all residuals were dissolved with a small amount of acetonitrile and precipitated by ether/methanol (v/v, 1:5, 0°C). The products were collected by centrifugation (10,000 rpm, 15 min), and this procedure of purification (dissolved and precipitated) was repeated for three times. Finally, the product was vacuum dried to constant weight at 35°C, and brown solid was obtained, which was stored at −20°C for later use.

2.3 Preparation of MNPs, Em-MNPs, and Cy7-Em-MNPs

Under vigorous string, 2 mL PLGA-b-mPEG solution (acetonitrile/tetrahydrofuran (THF) = 1:1, 100 mg/mL) was added to 2 mL proloxam 188 aqueous solution (50 mg/mL) at the rate of 0.5 mL/min. After acetonitrile was completely volatilized, MNPs were collected by centrifugation (6,600 rpm, 10 min) and washed with water for three times. When Em-MNPs and Cy7-Em-MNPs were prepared, Em or Cy7 was dissolved with PLGA-b-mPEG in acetonitrile/tetrahydrofuran (v/v = 1:1, 100 mg/mL), and then, Em or Cy7-Em-MNPs were prepared according to the preparation and the purification method of MNPs. Finally, MNPs, Em-MNPs, or Cy7-Em-MNPs were dispersed in saline or water and stored at 4°C for later use.

2.4 Determination of encapsulation efficiency (EE)

The content of Em in Em-MNPs was determined by the UV/visible spectrophotometer. First, lyophilized Em-MNPs (1 mg) were dissolved in the mixture of acetonitrile (LC-MS, 50 μL) and methanol (LC-MS, 500 μL). PLGA precipitation and Em were dissolved in methanol and centrifuged (13,000 rpm, 10 min). The centrifugation of

residue was repeated (dissolved – precipitated – centrifuged) for three times. Then, the upper liquid was concentrated in a new centrifuge tube (7 mL) and blow dried with nitrogen. Methanol (LC-MS) was added to dissolve the residue, with a constant volume of 50 mL. Finally, 2.0 mL Em methanol solution was removed with a 0.22 nm filter head, and the Em concentration was determined by the UV-vis spectrometer (Thermo Fisher Multiskan, Finland). Meanwhile, the EE and drug loading efficiency (DLE) of Em were calculated according to the following formulas:

$$\text{EE}\ (\%) = \frac{\text{Em amount in Em} - \text{MNPs}}{\text{Em adding amount}} \times 100\%. \quad (1)$$

$$\text{DLE}\ (\%) = \frac{\text{Em amount in Em} - \text{MNPs}}{\text{Quantity of MNPs}} \times 100\%. \quad (2)$$

2.5 *In vitro* stability and drug release of Em-MNPs

First, Em-MNPs were dispersed in phosphate buffered solution (PBS) (10 mM, pH 7.4), 10% FBS, and saline and placed in a constant temperature metal bath (37°C, 1,000 rpm). Then, 100 μL dispersion was extracted at different times (1, 3, 6, 12, 24, 48, 72, 120, and 168 h) for the determination of hydrodynamic diameter (HD) of Em-MNPs. Before HD of Em-MNPs was determined, the PBS and saline dispersions of Em-MNPs were diluted with 2 mL water, and the FBS dispersions of Em-MNPs were centrifuged (6,600 rpm, 15 min) to remove FBS, and then 2 mL water was added for dispersion. HD was characterized by quantity value.

The *in vitro* release of Em-MNPs was determined by dialysis [19]. Fetal bovine serum (FBS; 10%), renal tissue homogenate (10%), PBS (10 mM, pH 7.4), and saline were selected as dispersion and dialysate. The preparation method of renal tissue homogenate was as follows: twice the volume of saline (g/mL) was added to the kidney of C57BL/6 mice, and the kidney was homogenized with cell pulverizer. First, the concentration of Em-MNPs was made to be 2 mg/mL. 2 mL of Em-MNPS dispersions were placed in a dialysis bag (30 kDa) and placed in the corresponding dialytic solution (100 mL), which was stirred slowly at 37°C. Then, 1 mL dialysate was taken out at different time points (0.5, 1, 2, 4, 8, 12, and 24 h), 3 mL ethyl acetate (LC-MS) was added for extraction by rotating for 5 min, the mixture was centrifuged at 10,000 rpm for 5 min, and the upper organic extract was collected, which was repeated for three times. All the extraction liquid was blow dried with nitrogen, and the residue was added to methanol for dissolution and constant volume to 10 mL. Finally, 2.0 mL methanol solution was used to remove the large particles with a 0.22 μm filter head. The concentration of Em was determined by the UV-vis spectrometer, and the cumulative release rate of Em was calculated.

2.6 Cell uptake assay

MNPs were labeled with Cy7 to track the specificity of intracellular distribution. Normal rat kidney proximal tubular epithelial cells (NRK-52E, American Type Culture Collection, USA) were planted into coverslip at 37°C overnight and then incubated with Cy7 and Cy7-Em-MNPs (equivalent to 50 μg/mL emodin) for 2 h, respectively. Then, the medium was removed, and ice-cold PBS was added to wash the Cy7 and Cy7-Em-MNPs for three times. Then, the cell nuclear was stained with 4′,6-diamidino-2-phenylindole for 5 min in the dark. Epifluorescence microscope was used to analyze the cellular distribution of Em-MNPs.

2.7 Cytotoxicity assay

NRK-52E cells were cultured with Dulbecco's Modified Eagles's Medium containing 10% FBS, 100 U/mL penicillin, and 100 μg/mL streptomycin. Different concentrations of emodin and Em-MNPs solution from 5 to 50 μg/mL were added to 96-well plates for 12 and 24 h. Finally, the cell viability was evaluated using a cell counting CCK-8 kit and measured by Thermo Fisher Multiskan GO UV/visible spectrophotometer (Shimadzu, Japan) [20].

2.8 Kidney targeting evaluation

The animal protocol was approved by the Animal Ethics Committee of Nanfang Hospital. Balb/c mice were administrated with Cy7 and Cy7-Em-MNPs (equivalent to 1.0 mg/kg emodin) for 12 and 24 h, respectively. All mice were sacrificed at corresponding time, and then their major organs, namely, heart, liver, spleen, lung, kidneys, thymus, muscle, small intestine, and brain, were collected. Before fluorescence imaging, major

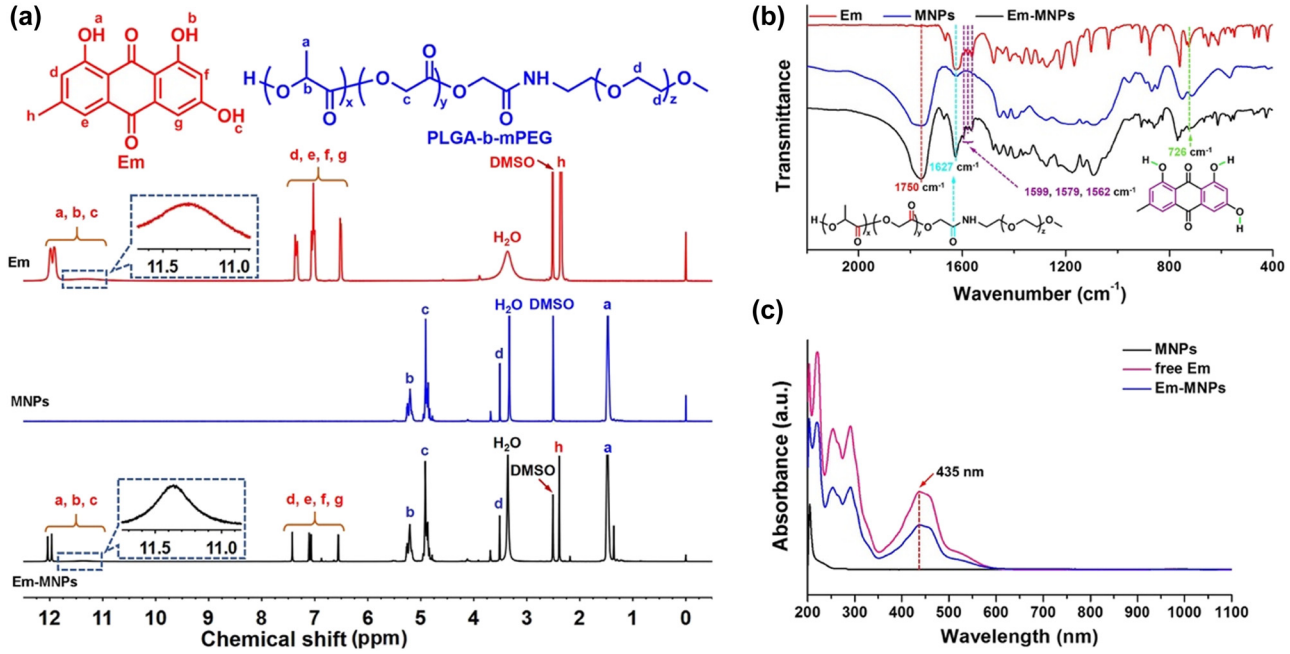

Figure 1: Characterization of MNPs and Em-MNPs. (a) ^{1}H NMP spectra of Em, MNPs, and Em-MNPs. (b) FTIR of the Em, MNPs, and Em-MNPs. (c) UV-vis spectra of MNPs, free Em, and Em-MNPs.

organs were washed with ice-cold PBS for three times to remove the surface fluorescence. After washing, fresh organs were placed on the glass plate to image with excitation at 710 nm and emission at 790 nm by the imaging system (Burker Imaging System, USA).

2.9 Pharmacodynamics study on renal unilateral ureteral obstruction (UUO) model

UUO models were performed based on the procedure demonstrated in the previous study [21]. 6–8 weeks mice were anesthetized using pentobarbital sodium (3%, 1.5 mL/kg, i.p.). All mice were randomly divided into four groups (n = 6 per group): (1) Sham group, (2) UUO + vehicle (PBS) group, (3) UUO + MNPs group, (4) UUO + Em-MNPs (equivalent to 1.0 mg/kg emodin). The mice were injected with corresponding drugs on the first day after operation and for 3 days. Then, all mice were sacrificed, and kidneys were collected for the following measurements.

After fixing with 10% neutral formaldehyde at 4°C overnight, kidneys were dehydrated, hyalinized, and embed for histology staining. 4 μm kidney slices were cut and stained with hematoxylin and eosin (H&E) staining to analyze the effect of Em-MNPs in the UUO mice model.

2.10 Statistical analysis

All experiments were performed for at least three times, and the data were collected. The statistical comparisons between groups were performed by t test using SPSS software (version 23.0). $P < 0.05$ was considered as statistically significant.

3 Results and discussion

3.1 Characterization of PLGA-b-mPEG and Em-MNPs

The structures of PLGA-b-mPEG and the encapsulation of Em were confirmed by ^{1}H nuclear magnetic resonance spectra, Fourier transform infrared (FTIR) and UV-vis spectra. As shown in Figure 1a, the chemical shift peaks at 2.1, 6.5–7.5 and 11.0–12.1 ppm of Em-MNPs were consistent with that of Em, and the peaks at 1.5, 3.5 and 4.9–5.3 ppm were consistent with that of PLGA-b-mPEG. Relative to FTIR spectra of Em-MNPs, there appeared obvious vibration peaks at 1,750 and 1,627 cm^{-1}, which were carboxyl characteristic vibration of PLGA-b-mPEG. Besides, the visible stretching vibration peaks of

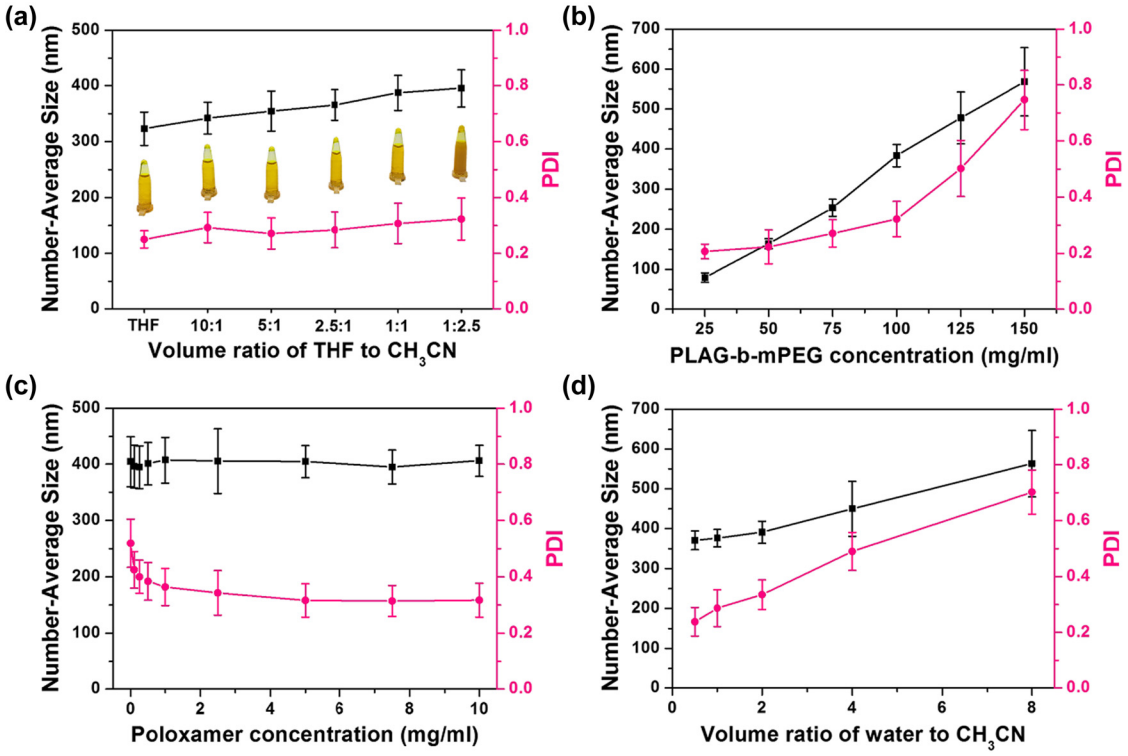

Figure 2: Optimization of the Em-MNPs. Hydrodynamic size of Em-MNPs prepared under different (a) volume ratios of THF to CH_3CN, (b) PLAG-b-mPEG concentration, (c) poloxamer concentration, and (d) volume ration of water to CH_3CN.

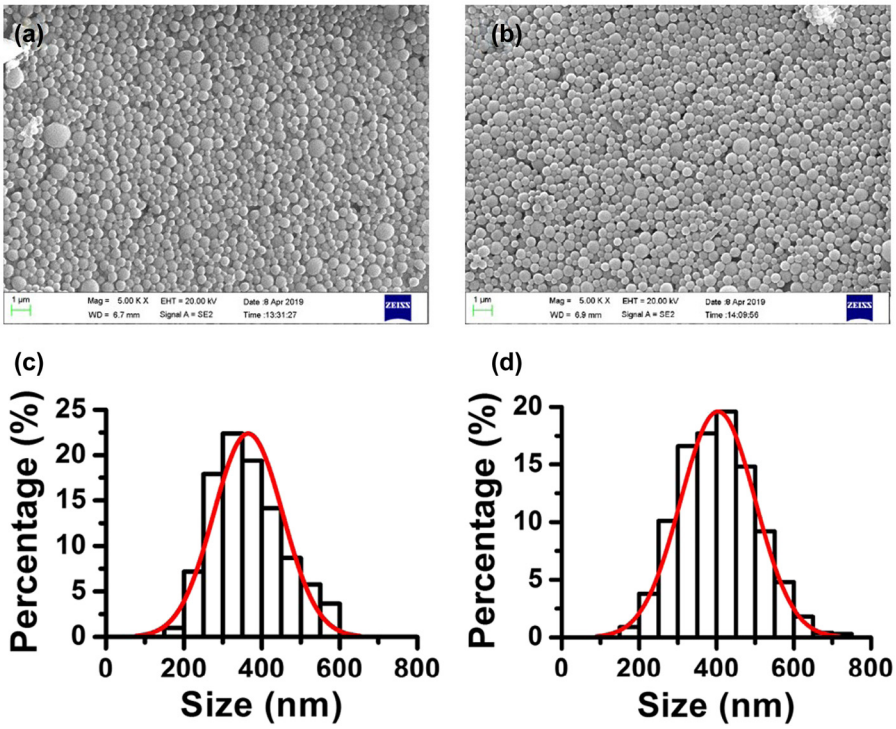

Figure 3: Morphology of MNPs and Em-MNPs. SEM images of MNPs (a) and Em-MNPs (b). Diameter distributions of MNPs (c) and Em-MNPs (d) counted in SEM images.

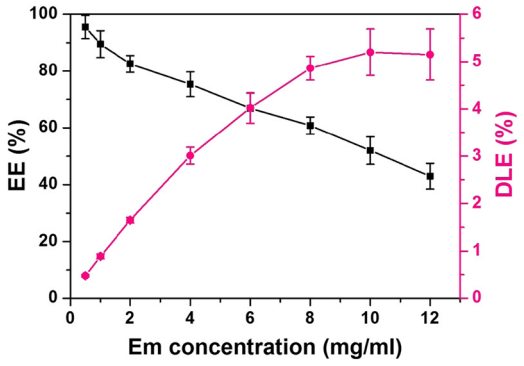

Figure 4: Encapsulation efficiency (EE) and drug loading efficiency (DLE). EE and DLE after adding different concentrations of Em (1–12 mg/mL).

benzene in Em-MNPs indicated that the Em had been encapsulated in NPs successfully (Figure 1b). This was further confirmed by UV-vis spectra (Figure 1c). These three methods were favorable measurements to verify the linkage of Em with MNPs, which was also used in other studies [22,23].

3.2 Optimization of the Em-MNPs fabrication

Em-MNPs were prepared by a simple nanometer precipitation method, in which Poloxam 188 was used as a surfactant to stabilize Em-MNPs. The size and the homogeneity of Em-MNPs can be adjusted by changing PLGA-b-mPEG concentration, poloxam 188 concentration, and aqueous/solvent phase volume ratio. Figure 2a shows the hydrodynamic size (HD) and polydispersity index (PDI) of Em-MNPs prepared under different organic solvent ratio. Along with the decreasing of THF, the particle size gradually increased, while the PDI for each sample kept steady. However, with the increase of PLGA-b-mPEG concentration, the HD and PDI of Em-MNPs increased significantly, which reached the high concentration of PLGA-b-mPEG went against to the monodispersion of NPs (Figure 2b). The effect of poloxam 188 on particle size and dispersion was negligible (Figure 2c), while the proportion of organic solvent showed great influence on the particle size (Figure 2d). Therefore, the optimal condition for the preparation of Em-MNPs was as follows: 100 mg/mL PLGA-b-mPEG, 50 mg/mL Proloxam 188, and the volume ratio of aqueous/solvent phase 1.0.

Then, the morphology of MNPs and Em-MNPs was observed by scan electronic microscope (SEM). As shown in Figure 3, the as-prepared NPs were uniform spheres. The diameter observed from SEM images of Em-MNPs (394.0 ± 71.4 nm) was slightly larger than that of MNPs (361.3 ± 74.9 nm), and the HD for Em-MNPs was also greater than MNPs, indicating that the Em encapsulation enlarged the size of MNPs and the hydration layer on the surface of NPs enhanced this trend. It is worth noting that the EE and DLE were closely related to the amount of Em added. As shown in Figure 4, the EE decreased along with the increased Em concentration, while the DLE was proportionate to the Em concentration. When the Em concentration was 6 mg/mL, the EE and DLE reached a balance of 66.9% and 4.0%, respectively. The cross point of EE and DLE indicated that the concentration of Em added has reached an optimal value with relatively high drug loading amount and efficiency.

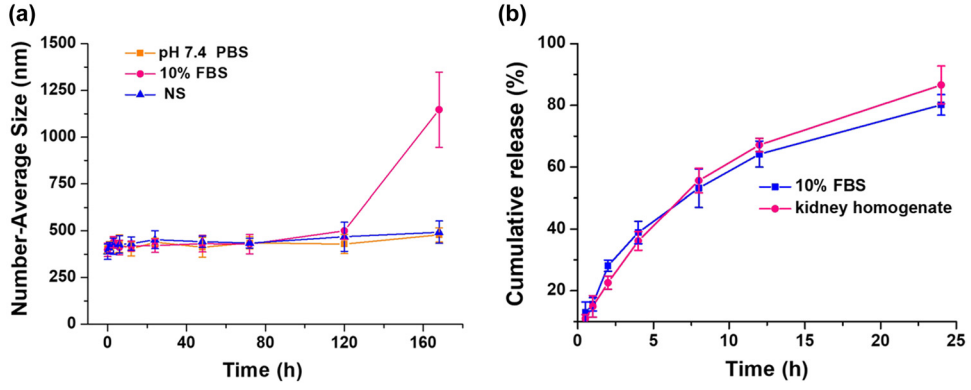

Figure 5: Stability and *in vitro* release assays of Em-MNPs in different media. The stability of Em-MNPs (a) measured by HD in PBS (pH 7.4), 10% FBS, and saline (NS) at 37°C. *In vitro* release assay of Em released from Em-MNPs (b) in 10% FBS and kidney homogenate at 37°C.

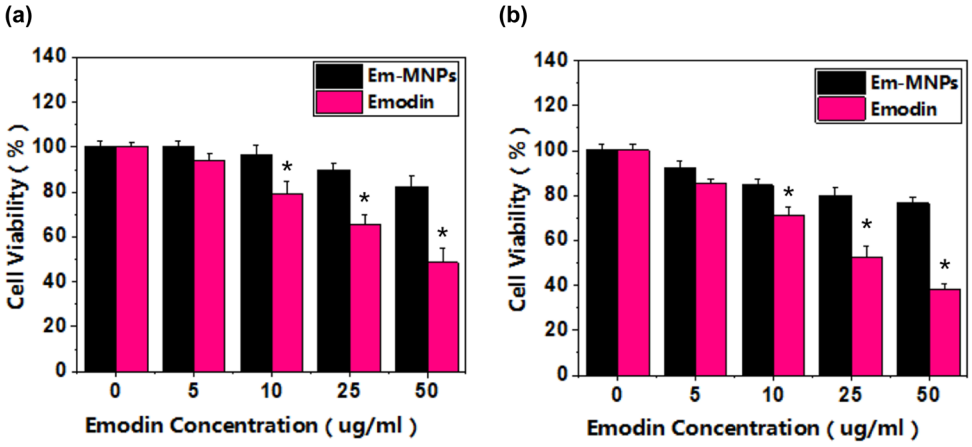

Figure 6: Cytotoxicity assay. Cell viability of rat proximal tubular cells treated with emodin (0–50 μg/mL) and Em-MNPs (equivalent to 0–50 μg/mL emodin) for 12 h (a) and 24 h (b), respectively. *$p < 0.05$ versus the Em-MNPs group.

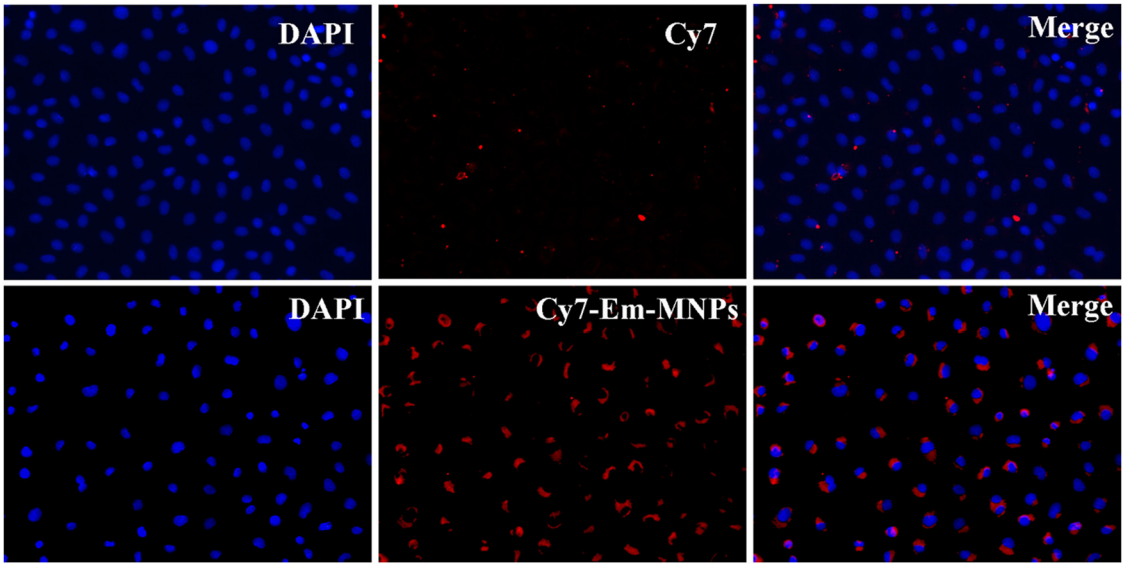

Figure 7: Cellular uptake images. NRK-52E cells incubated with Cy7 and Cy7-Em-MNPs for 2 h. Images were captured in 400× magnification.

3.3 Stability and *in vitro* release assays

To further investigate the stability of Em-MNPs in different media, HDs of Em-MNPs were measured after incubation with PBS (10 mM, pH 7.4), saline, and 10% FBS at different time points. As shown in Figure 5a, the HDs of Em-MNPs were stable up to 7 days when Em-MNPs were incubated with PBS and saline. After treated with FBS, a medium enriched with proteins, the HD of Em-MNPs was nearly same to that of the initial condition at 5 days. As reported in the recent study, the HD of Em-MNPs remained stable for 2.5 times longer than MNPs [24]. *In vitro* release assay was conducted in 10% FBS and kidney homogenate at 37°C. With the increasing time, Em exhibited a high release profile from the Em-MNPs in those two media (Figure 5b). The cumulative release rate reached 80.2% and 86.6% in the FBS and kidney homogenate for 24 h, respectively. Compared to covalent modification, Em-MNPs showed higher drug release rate [25], thereby releasing Em from Em-MNPs and improving drug efficacy.

3.4 Cellular uptake study

Cy7 and Cy7-Em-MNPs were used to observe the intracellular uptake efficiency. Figure 6 shows the fluorescence imaging distribution of NRK-52E cells

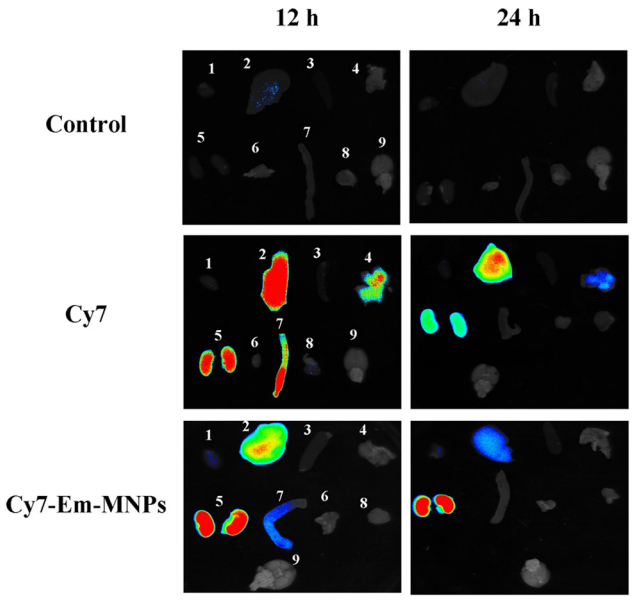

Figure 8: *Ex vivo* fluorescence imaging. Balb/c mice injected with PBS (control), and Cy7 and Cy7-Em-MNPs for 12 h and 24 h, respectively and major organs were collected for imaging. 1, heart; 2, liver; 3, spleen; 4, lung; 5, kidney; 6, thymus; 7, small intestine; 8, muscle; 9, brain.

treated with PBS, Cy7, and Cy7-Em-MNPs, respectively. After incubation for 2 h, the fluorescence signal of Cy7-Em-MNPs was significantly stronger than that of free Cy7. It was suggested that the accumulation of Cy7-Em-MNPs was much higher than that of Cy7. The Cy7-Em-MNPs were mainly distributed around nucleus, thereby suggesting that Cy7-Em-MNPs were mainly located and released drugs in the cytoplasm rather than nucleus. Accordingly, these data indicated that Em-MNPs had higher uptake efficiency *in vitro* and might be suitable for kidney diseases. The possible endocytic mechanism was the protonation of the surface of Em-MNPs, coinciding with triptolide-encapsulated MNPs [17], which resulted in endosome rupture and then realized lysosome escape [26]. Besides, Williams et al. also demonstrated that free MNPs performed good cellular uptake and biocompatibility [24].

3.5 Cytotoxicity assay

To compare the cytotoxicity of emodin and Em-MNPs, NRK-52E cells were treated with emodin and Em-MNPs in different concentration gradients (5–50 μg/mL) for 12 and 24 h, respectively (Figure 7). The viability of cells was measured by CCK-8, which is a classical method to evaluate cell toxicity of nanomaterials [27]. When cells incubated with free emodin at the concentration of 10 μg/mL, cell viability presented significant suppression. With the increasing concentration of emodin, the toxicity of emodin grow sharply after incubation for 24 h. However, the viability of cells treated with Em-MNPs were maintained in relative high levels (>85%). This result suggested that loading emodin with MNPs could significantly decrease the cytotoxicity of emodin. Moreover, our previous study found that MNPs reduced the toxicity of triptolide in other three cell lines [17] and further demonstrated that MNPs could serve as promising drug carriers with good biocompatibility.

3.6 Kidney targeting capacity

To further examine the kidney targeting capacity of Cy7-Em-MNPs, an *ex vivo* tissue localization was performed at 12 h and 24 h in Balb/c mice (Figure 8). As a result, Cy7-Em-MNPs was mostly accumulated in kidneys rather than other organs (heart, liver, spleen, and lung) after injection for 12 h. With the increasing time, the fluorescence density was increased in kidneys of Cy7-Em-MNPs. However, free Cy7 treated kidneys had no apparent fluorescence retention during the period, indicating that Cy7-Em-MNPs had favorable renal retention ability. The slit diaphragm of podocytes (the molecular barrier of the nephron, ~40 nm) are too small for Em-MNPs to pass through [28,29]. So, the kidney-targeting mechanism of MNPs might be attributed to the endothelial cells of the peritubular in the kidneys, which also verified that excellent kidney-targeting capability of free MNPs [24]. The pressure in the nephron and the reabsorption ability of peritubular capillaries induced endocytosis of Cy7-Em-MNPs in kidney tubular cells. Therefore, Cy7-Em-MNPs was an excellent option for the following pharmacodynamics analysis in the animal model.

3.7 Pharmacodynamics study

UUO mice were a well-recognized and classical animal model of chronic kidney fibrosis [30]. So, the therapeutic effect of Em-MNPs was performed in the UUO model. Figure 9 depicts histology characteristics in different treatment groups for H&E staining. The ligated kidney in UUO mice showed apparent tubular dilation, lumen disappear, fibrosis, and increased inflammatory cells [31]. After treating with Em-MNPs, the manifestation of

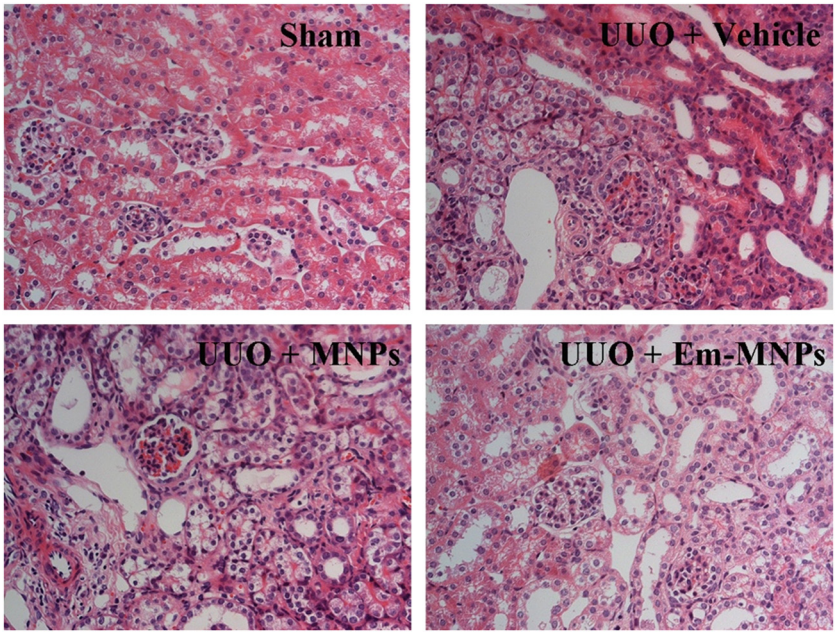

Figure 9: Histology analysis of kidneys. H&E staining images of kidneys from sham-operated, UUO + Vehicle (PBS), UUO + MNPs, and UUO + Em-MNPs mice.

ligated kidney was significantly alleviated, which characterized as decreased inflammation cells and less matrix accumulation in the tubulointerstitium. These results revealed that Em-MNPs could specifically treat kidney injury, which might be ascribed to the targeting ability and long retention of Em-MNPs in kidneys. Furthermore, UUO mice treated with free MNPs could not perform the therapeutic effects, suggesting that the effects of Em-MNPs mainly was derived from emodin.

4 Conclusion

In summary, we successfully designed monodispersed MNPs and loaded with emodin (Em-MNPs). Em-MNPs possessed low toxicity, high cell uptake efficiency, kidney-targeting ability, and long retention time in the kidneys. In the UUO model, Em-MNPs presented excellent antifibrosis effects and may represent a potential strategy for the treatment of renal diseases.

Acknowledgments: This study was supported by the China Postdoctoral Science General Foundation (Nos.2018M643138, 2018M643135), "San-ming" Project of Medicine in Shenzhen (No. SZSM201812097), the National Natural Science Foundation of China (Grants 81770727, 21673081), GDUPS (2017), Key Project of Guangzhou Science Technology and Innovation Commission (201804020054), Key Project of Guangdong Natural Science Foundation (2018B030311002), and Key Project Science and Technology Planning Project of Guangdong Province (2017A010103041).

Conflict of interest: The authors declare no conflict of interest.

References

[1] Liu Y, Workalemahu B, Jiang XY. The effects of physicochemical properties of nanomaterials on their cellular uptake *in vitro* and *in vivo*. Small. 2017;13(43):1701815.
[2] Chen A, Chatterjee S. Nanomaterials based electrochemical sensors for biomedical applications. Chem Soc Rev. 2013;42(12):5425–38.
[3] Smith BR, Gambhir SS. Nanomaterials for *in vivo* imaging. Chem Rev. 2017;117(3):901–86.
[4] Nicolas J, Mura S, Brambilla D, Mackiewicz N, Couvreur P. Design, functionalization strategies and biomedical applications of targeted biodegradable/biocompatible polymer-based nanocarriers for drug delivery. Chem Soc Rev. 2013;42(3):1147–235.
[5] Santoro M, Shah SR, Walker JL, Mikos AG. Poly(lactic acid) nanofibrous scaffolds for tissue engineering. Adv Drug Deliv Rev. 2016;107:206–12.
[6] Zhao N, Yan L, Zhao X, Chen X, Li A, Zheng D, et al. Versatile types of organic/inorganic nanohybrids: from strategic design to biomedical applications. Chem Rev. 2019;119(3):1666–762.

[7] Ling DS, Hackett MJ, Hyeon T. Surface ligands in synthesis, modification, assembly and biomedical applications of nanoparticles. Nano Today. 2014;9(4):457–77.
[8] Zhang L, Wang F, Wang L, Wang W, Liu B, Liu J, et al. Prevalence of chronic kidney disease in China: a cross-sectional survey. Lancet. 2012;379(9818):815–22.
[9] Tampe D, Zeisberg M. Potential approaches to reverse or repair renal fibrosis. Nat Rev Nephrol. 2014;10(4):226–37.
[10] Zhong Y, Menon MC, Deng Y, Chen Y, He JC. Recent advances in traditional Chinese medicine for kidney disease. Am J Kidney Dis. 2015;66(3):513–22.
[11] Yuan XP, He XS, Wang CX, Liu LS, Fu Q. Triptolide attenuates renal interstitial fibrosis in rats with unilateral ureteral obstruction. Nephrology. 2011;16(2):200–10.
[12] Li X, Liu W, Wang Q, Liu P, Deng Y, Lan T, et al. Emodin suppresses cell proliferation and fibronectin expression via p38MAPK pathway in rat mesangial cells cultured under high glucose. Mol Cell Endocrinol. 2009;307(1–2):157–62.
[13] Wang S, Chen T, Chen R, Hu Y, Chen M, Wang Y. Emodin loaded solid lipid nanoparticles: preparation, characterization and antitumor activity studies. Int J Pharm. 2012;430(1–2):238–46.
[14] Daraee H, Eatemadi A, Abbasi E, Fekri Aval S, Kouhi M, Akbarzadeh A. Application of gold nanoparticles in biomedical and drug delivery. Artif Cell Nanomed Biotechnol. 2016;44(1):410–22.
[15] Kroger APP, Paulusse JMJ. Single-chain polymer nanoparticles in controlled drug delivery and targeted imaging. J Control Rel. 2018;286:326–47.
[16] Qiao H, Sun M, Su Z, Xie Y, Chen M, Zong L, et al. Kidney-specific drug delivery system for renal fibrosis based on coordination-driven assembly of catechol-derived chitosan. Biomaterials. 2014;35(25):7157–71.
[17] Deng X, Zeng T, Li J, Huang C, Yu M, Wang X, et al. Kidney-targeted triptolide-encapsulated mesoscale nanoparticles for high-efficiency treatment of kidney injury. Biomater Sci. 2019;7(12):5312–23.
[18] Cheng J, Teply BA, Sherifi I, Sung J, Luther G, Gu FX, et al. Formulation of functionalized PLGA-PEG nanoparticles for *in vivo* targeted drug delivery. Biomaterials. 2007;28(5):869–76.
[19] Huang C, Zeng T, Li J, Tan L, Deng X, Pan Y. Folate receptor-mediated renal-targeting nanoplatform for the specific delivery of triptolide to treat renal ischemia/reperfusion injury. ACS Biomater Sci Eng. 2019;5(6):2877–86.
[20] Geng X, Zhang M, Lai X, Tan L, Liu J, Yu M, et al. Small-sized cationic miRi-PCNPs selectively target the kidneys for high-efficiency antifibrosis treatment. Adv Healthc Mater. 2018;7(21):e1800558.
[21] Tan L, Lai X, Zhang M, Zeng T, Liu Y, Deng X, et al. A stimuli-responsive drug release nanoplatform for kidney-specific anti-fibrosis treatment. Biomater Sci. 2019;7(4):1554–64.
[22] Ye P, Wei S, Luo C, Wang Q, Li A, Wei F. Long-term effect against methicillin-resistant *Staphylococcus aureus* of emodin released from coaxial electrospinning nanofiber membranes with a biphasic profile. Biomolecules. 2020;10(3):362.
[23] Song Y, Sheng Z, Xu Y, Dong L, Xu W, Li F, et al. Magnetic liposomal emodin composite with enhanced killing efficiency against breast cancer. Biomater Sci. 2019;7(3):867–75.
[24] Williams RM, Shah J, Ng BD, Minton DR, Gudas LJ, Park CY, et al. Mesoscale nanoparticles selectively target the renal proximal tubule epithelium. Nano Lett. 2015;15(4):2358–64.
[25] Yuan ZX, Wu XJ, Mo J, Wang YL, Xu CQ, Lim LY. Renal targeted delivery of triptolide by conjugation to the fragment peptide of human serum albumin. Eur J Pharm Biopharm. 2015;94:363–71.
[26] Zhu D, Yan H, Zhou Z, Tang J, Liu X, Hartmann R, et al. Detailed investigation on how the protein corona modulates the physicochemical properties and gene delivery of polyethylenimine (PEI) polyplexes. Biomater Sci. 2018;6(7):1800–17.
[27] Chen X, Feng B, Zhu DQ, Chen YW, Ji W, Ji TJ, et al. Characteristics and toxicity assessment of electrospun gelatin/PCL nanofibrous scaffold loaded with graphene *in vitro* and *in vivo*. Int J Nanomed. 2019;14:3669–78.
[28] Johnstone DB, Holzman LB. Clinical impact of research on the podocyte slit diaphragm. Nat Clin Pract Nephrol. 2006;2(5):271–82.
[29] Weavers H, Prieto-Sánchez S, Grawe F, Garcia-López A, Artero R, Wilsch-Bräuninger M, et al. The insect nephrocyte is a podocyte-like cell with a filtration slit diaphragm. Nature. 2009;457(7227):322–6.
[30] Baues M, Klinkhammer BM, Ehling J, Gremse F, van Zandvoort M, Reutelingsperger CPM, et al. A collagen-binding protein enables molecular imaging of kidney fibrosis *in vivo*. Kidney Int. 2020;97(3):609–14.
[31] Bi J, Watanabe H, Fujimura R, Nishida K, Nakamura R, Oshiro S, et al. A downstream molecule of 1,25-dihydroxy-vitamin D3, alpha-1-acid glycoprotein, protects against mouse model of renal fibrosis. Sci Rep. 2018;8(1):17329.